The Flatness of Lamellipodia Explained by the Interaction Between Actin Dynamics and Membrane Deformation

Christian Schmeiser[a,b], **Christoph Winkler**[b,1]

[a] Faculty of Mathematics, University of Vienna, Oskar-Morgenstern-Platz 1, 1090 Vienna, Austria.
[b] Johann Radon Institute for Computational and Applied Mathematics, Austrian Academy of Sciences, Altenberger Straße 69, 4040 Linz, Austria.

[1] Corresponding author at: Johann Radon Institute for Computational and Applied Mathematics, Austrian Academy of Sciences,
Altenberger Straße 69, 4040 Linz, Austria.
Email address: christoph.winkler@ricam.oeaw.ac.at

Abstract

The crawling motility of many cell types relies on lamellipodia, flat protrusions spreading on flat substrates but (on cells in suspension) also growing into three-dimensional space. Lamellipodia consist of a plasma membrane wrapped around an oriented actin filament meshwork. It is well known that the actin density is controlled by coordinated polymerization, branching, and capping processes, but the mechanisms producing the small aspect ratios of lamellipodia (hundreds of nm thickness vs. several μm lateral and inward extension) remain unclear.

The main hypothesis of this work is a strong influence of the local geometry of the plasma membrane on the actin dynamics. This is motivated by observations of co-localization of proteins with I-BAR domains (like IRSp53) with polymerization and branching agents along the membrane. The I-BAR domains are known to bind to the membrane and to prefer and promote membrane curvature. This hypothesis is translated into a stochastic mathematical model where branching and capping rates, and polymerization speeds depend on the local membrane geometry and branching directions are influenced by the principal curvature directions. This requires the knowledge of the deformation of the membrane, being described in a quasi-stationary approximation by minimization of a modified Helfrich energy, subject to the actin filaments acting as obstacles. Simulations with this model predict pieces of flat lamellipodia without any prescribed geometric restrictions.

Key words: lamellipodium, actin filament, finite element
MSC: 92C10, 92C17

1 Introduction

Movement of individual animal cells is almost exclusively performed by crawling locomotion [1], and plays a major role in a huge variety of physiological processes, i.e. embryogenesis [30, 24], immune interaction [23, 34], the formation and transformation of the nervous system [44, 67], and tumor invasion [32, 37].

On flat surfaces, adhesive crawling of many cell types is based on lamellipodia, which are thin (100–200 nm) but wide (up to several μm), sheet-like cell protrusions [56]. Their flat shape is not necessarily caused by flat substrates, since they are also observed on non-adhesive cells like leukocytes in suspension [68]. Lamellipodia consist of a highly organized actin filament network, wrapped by the cell membrane [7, 61].

The membrane envelopes the cell and forms the barrier between the interior of the cell and its environment (reviewed in [12]). It consists of a bilayer of phospholipids which can move freely within their sheets [15], making plasma membranes behave like two-dimensional fluids. Specific functionalities are enabled by certain proteins that get attached to the plasma membrane in various ways [62, 6]. Important for our study is that some of these membrane proteins are able to sense and/or create curvature in the membrane (reviewed in [38]).

The structure protein actin is found in almost all eukaryotic cells and many prokaryotes (reviewed in [47]). It can bind to other actin monomers in a head-to-tail fashion [65] and is therefore able to form long, double-helical filaments [20] with a diameter of appoximately 7nm. The polarity gives the filament an orientation, with the preferentially growing end called the plus- or barbed end, and the other, predominantly shrinking one, the minus- or pointed end. Actin filaments are much more flexible than microtubules [18], another part of the cytoskeleton. So in order to create more stable structures, over one hundred accessory proteins help to regulate actin monomers and filaments. The formation and rebuilding of actin filament networks in lamellipodia is influenced by the following processes [41]:

- Polymerization: The most important polymerization mechanisms are those promoted by formin or members of the VASP or WASP families occurring at barbed ends abutting the cell membrane. Most likely these proteins also provide tethering of barbed ends to membrane proteins (and, thus, to the cell membrane) they are binding to [8].

- Branching: From existing mother filaments, new daughter filaments can be nucleated by the Actin-Related Protein-2/3 (Arp2/3) complex, branching off at an angle of approximately 70 degrees. Arp2/3 itself is activated at the membrane by nucleation-promoting-factors (NPFs), such as the Wiskott-Aldrich syndrome protein (WASP) or Scar/Wave [33].

- Capping: The binding of Capping Protein (CP) to the barbed end of a filament blocks the further polymerization und thus stops the elongation process [64]. Filaments attached to an end-tracking motor are protected from capping.

The architecture of the filament network is also influenced by cross-linking proteins (e.g. α-actinin, Fascin, Filamin [59]), breaking of actin filaments by the severing protein Gelsolin [5], adhesions to the substrate [46], and depolymerization of actin filaments, e.g. by the Actin Depolymerizing Factor (ADF/Cofilin) [3]. These processes are, however, less important for the present study of steadily protruding lamellipodia, where the relative movement of the filaments and thus the effects of cross-linking and adhesions can be neglected. The filament decomposition mechanisms do not significantly affect the lamellipodium geometry either, and will not be discussed further.

The polymerization of barbed filament ends is pushing the plasma membrane outward. The shape of the resulting protrusion mostly depends on the regulation of polymerization, branching, and capping. However, a more direct interaction with membrane shape might be due to the way signalling molecules, regulating the polymerization and branching machinery, are imbedded in [2] or bound to [55] the membrane. There is strong evidence for the relevance of the latter for filopodium and lamellipodium protrusion. The insulin receptor tyrosine kinase substrate of 53 kdA (IRSp53) seems to be especially important, reviewed in [55], as it links membrane curvature with its membrane binding, 'zeppelin'-shaped I-BAR domain to polymerization and branching activity, by binding via its SH3 domain to polymerization promotors and to the branching activator WAVE and thus generating a positive feedback loop. The details of these processes are unknown, and it is one of the main contributions of the present work to formulate a model for the IRSp53 mediated interaction between membrane deformation and actin dynamics, where the unknown details are filled in in a way, which is consistent with experimental evidence as well as with basic geometric and mechanical considerations.

The first assumption is that IRSp53 is localized at the membrane and that its localization within the membrane is driven by a preference for highly curved regions. This can be justified by energy considerations using the shape and membrane binding properties of the I-BAR domain (analogously to [2]). As a second premise it is assumed that IRSp53 molecules form clusters, a property that is indicated by the large scale deformations of membranes [51]. It will be assumed that a cluster with the shape of a band attached to the membrane is running along the leading edge, which induces membrane curvature (orthogonal to the direction of the band) according to the shape of the I-BAR domain of IRSp53. The third assumption is that the machineries for polymerization and branching of actin filaments

co-localize with IRSp53, which is supported by experimental evidence [43]. For polymerization we adopt the actoclampin model [11, 10], based on end-tracking motors, with a force dependent polymerization speed. This has the consequence that polymerizing barbed ends are (via IRSp53) tethered to the membrane and protected from capping. A tether is supposed to have linear elastic stretching properties up to a threshold force, above which the tether breaks. As a logical consequence of the assumptions so far, the tether also breaks, when (by lateral or upward flow) the barbed end of the filament moves into a membrane region with no residence of IRSp53. It is assumed that untethered barbed ends continue to polymerize until they get capped, but are unable to nucleate new filaments. These properties are also present in the tethered ratchet model [40] where, however, the breaking of tethers occurs spontaneously and only untethered filaments polymerize until they are capped. We conjecture that with an appropriate choice of the relevant parameters the main qualitative properties of our model would be similar with a tethered ratchet submodel for polymerization.

Branching is assumed to happen at (or very close to) barbed ends with a fixed branching angle (here taken to be 73° [63]). The main question is to determine the direction of the plane spanned by mother and daughter filaments. Our choice is a consequence of the observation that IRSp53 is often observed in tubular structures [36]. Therefore we assume that it tends to line up in the direction of the smaller principal curvature of the membrane. This is translated to a preference of the daughter filament for this direction. Evidence for a preferred direction of branching is provided by data of [63] showing that smaller distances between branch points on actin filaments are approximately integer multiples of their helical pitch.

A precise mathematical formulation of the model will be given in the following section. It also requires a description of the membrane shape as a two-dimensional surface. This will be based on the well established Helfrich model [19], where the total bending energy of the membrane is minimized. The model has to be adapted to the present situation, with the actin filaments as obstacles and the possibility of inward pulling forces exerted by tethered barbed ends.

Mathematical models of lamellipodium dynamics roughly belong to one of two categories: 'Macroscopic' models consider the actin network as a continuum with various assumptions on filament geometry and/or the rheological properties of the network, e.g. [45, 50, 13]. The model used here belongs to the class of 'microscopic' models, where the dynamics of individual actin filaments are described (usually as stochastic processes). Simulations with microscopic models are typically restricted to lamellipodial segments close to the leading edge, both for complexity reasons and for a lack of detailed models for the events in the rear part and at the sides of the lamellipodium. Because of the flatness of lamellipodia, useful information on the network architecture can be obtained from two-dimensional models both with rigid

[63] and deformable leading edges [52]. The three dimensional network architecture has been investigated in this way with a prescribed rigid shape of the plasma membrane [54, 2] and with a deformable leading edge geometry [22]. In these studies, the basic flat shape of the lamellipodium including its thickness has been prescribed.

The model presented here seems to be the first without a priori information on lamellipodium geometry. Mathematically and numerically, this comes at the price of solving for the membrane a general two-dimensional time-dependent surface equation in three-dimensional space. Since the derivation and implementation of a suitable simulation algorithm has been a formidable challenge by itself, it is only outlined in the following section, and described in detail in a parallel work [53]. The important advantage of the model is a complete account for the interaction between membrane geometry and actin filaments. The simulation results presented in Section 3 show that the model predicts the development of flat lamellipodia. Also the computed architecture of the actin filament network agrees qualitatively with EM data. The simulations have been carried out with parameter values, which partially have been reported in the literature and partially are reasonable guesses. We are confident that a full parametrization of the model is possible by detailed comparisons to electron tomograms, similarly to [63]. This is the subject of ongoing work.

2 The mathematical model

The model consists of two interacting systems. The dynamics comes from the growth of actin filaments as they push (and sometimes pull) the membrane, which reacts passively and in a quasi-stationary way. However, there is a feedback effect by the influence of the membrane deformation on the actin dynamics.

Our model describes a small section of the lamellipodium close to the leading edge. Thus, artificial lateral and rear boundaries have to be introduced. Since our main goal is to explain the flatness of the lamellipodium, we have to be careful not to enforce the flatness by the data of the model. In particular, this could happen by the necessary inflow of filaments through the artificial lateral boundaries by lateral flow. The necessity of providing this data is avoided by a periodicity assumption, where the ouflow data at the left are the inflow data at the right and vice versa. The direction of periodicity will be orthogonal to the main protrusion direction. However, there is no restriction with respect to the other two directions such that the cross section and, in particular, the thickness of the growing structure is not restricted.

The plasma membrane

We model a piece of membrane which, when stretched out, is of roughly rectangular shape with two opposing boundary segments being the top and bottom parts of the rear boundary, and the other two the left and right part of the lateral boundary. The latter two will be mathematically identified by the periodicity assumption mentioned above. This means that our model resides in the domain $\mathbb{T}^1 \times \mathbb{R}^2$, where the one-dimensional torus $\mathbb{T}^1$ will be represented by the interval $[0, L_1]$, where $L_1 = x_{max}$ is roughly the length of the modelled piece of leading edge. Since we shall describe a membrane piece of fixed area A_0 (see below), it is natural to use the parameter space $S = \mathbb{T}^1 \times [0, L_2]$ with $L_2 = A_0/x_{max}$ for the parametrization

$$\mathscr{M}(t) = \{\mathbf{r}(\mathbf{s}, t) : \mathbf{s} \in S\} \subset \mathbb{T}^1 \times \mathbb{R}^2 ,$$

of the membrane piece at time $t \geq 0$.

The periodicities in parameter space and physical space are related by

$$\mathbf{r}(s_1 + L_1, s_2, t) = (r_1(\mathbf{s}, t) + x_{max}, r_2(\mathbf{s}, t), r_3(\mathbf{s}, t)) .$$

The rear boundary $\Gamma_r(t) := \mathbf{r}(\mathbb{T}^1 \times \{0, L_2\}, t)$ consists of the bottom and top parts with $s_2 = 0$ and, respectively, $s_2 = L_2$. The parametrization is only a geometric description of the membrane, and the parameter $\mathbf{s}$ does not have any physical meaning regarding the position of individual lipids. In particular, we do not attempt to describe the lipid flow along the membrane, which would significantly increase the complexity of the model [21], not necessary for the purpose of this work. The part of the membrane attached to the IRSp53 cluster (from now on called the *leading edge*) corresponds to the rectangle $S_{\mathscr{L}} := \mathbb{T}^1 \times [L_2/2 - L/2, L_2/2 + L/2]$ of width L in parameter space (see Fig. 1A):

$$\mathscr{L}(t) := \{\mathbf{r}(\mathbf{s}, t) : \mathbf{s} \in S_{\mathscr{L}}\} \subset \mathscr{M}(t) , \qquad t \geq 0 .$$

By the properties of IRSp53, the leading edge will have mechanical properties (described below) different from the rest of the membrane. Its location in physical space will be a result of the curvature distribution along the membrane.

At each point in time, the deformation of the membrane will be determined by minimization of a potential energy functional, subject to a number of constraints. These are partly due to the presence of the actin filaments, which are assumed to be rigid and immotile. Filaments will be labelled by the indices $i \in I(t) = \{1, \ldots, N(t)\}$, where $N(t) \in \mathbb{N}$ increases by one at each branching event. Since depolymerization and severing effects are not modelled, the activity of each filament can be described in terms of its (time independent) direction $\mathbf{f}_i \in S^2$ (i.e. $|\mathbf{f}_i| = 1$, oriented towards its barbed end) and of the position $\mathbf{F}_i(t)$ of the barbed end (satisfying

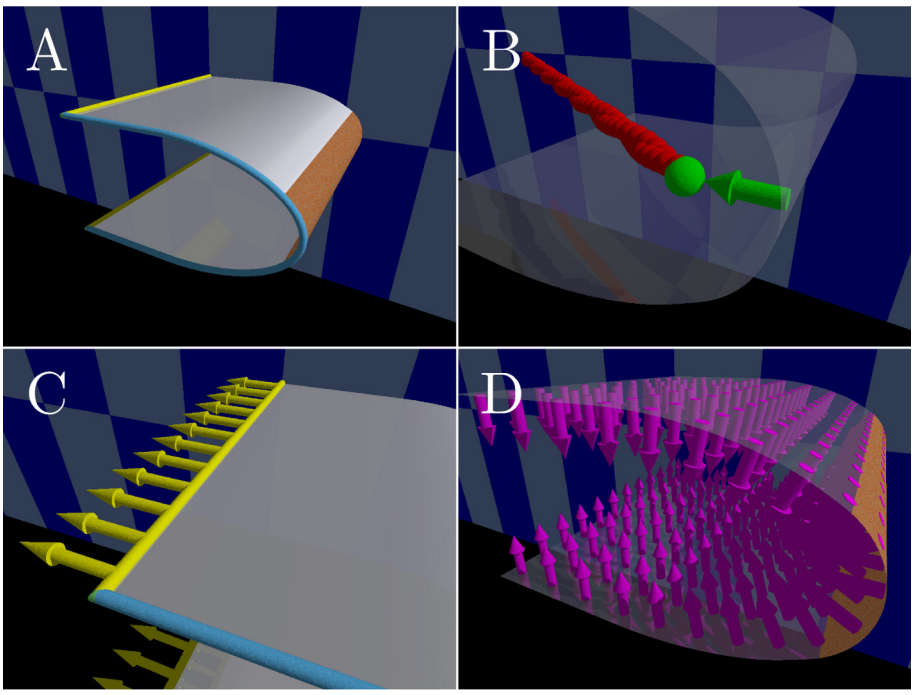

Figure 1: Membrane geometry and forces. A: Membrane geometry. The leading edge region $\mathscr{L}$ is depicted in brown, while the rest of the membrane is colored in silver. The rear boundary Γ_r and the lateral boundary at x_{max} are highlighted as yellow and, respectively, light blue tubes. The background wall functions as a reference only, with vertical stripes of width 100nm. B: Tether force. The linkage between the filament (depicted in red with a green barbed end) and the membrane (transparent) pulls the membrane back. The force is visualized by the green arrow. C: Membrane tension. The membrane tension (yellow) acts tangentially. D: Volume constraint force. For $\mu_{vol} > 0$ the inward pushing force (magenta) is acting on the whole membrane.

$\mathbf{F}_i(t_1) - \mathbf{F}_i(t_2) = \mathrm{sgn}(t_1 - t_2)|\mathbf{F}_i(t_1) - \mathbf{F}_i(t_2)|\mathbf{f}_i)$. We also distinguish between filaments whose barbed ends are tethered to the membrane, $i \in I_t(t)$, untethered, $i \in I_u(t)$, or capped, $i \in I_c(t)$, with $I(t) = I_t(t) \cup I_u(t) \cup I_c(t)$.

The bending energy: Plasma membranes behave like two-dimensional fluids [1], and can be described mechanically as deformable fluid surfaces [16]. They are virtually inextensible and cannot sustain shear stress, which makes bending the sole form of deformation.

We consider an adapted version of the Helfrich model [19], i.e. the Willmore functional

$$E_{bend}[\mathscr{M}] := 2\mu_{bend} \int_{\mathscr{M}} H^2 d\sigma \,, \tag{1}$$

with the bending modulus μ_{bend}, the surface area element $d\sigma$ on $\mathscr{M}$ and

the mean curvature $H = \frac{k_1+k_2}{2}$, where $k_1 \leq k_2$ are the signed principal curvatures with the convention that $k_j > 0$ corresponds to convexity of the cell. Compared to the full Helfrich energy, the Gauss curvature has been neglected, which is not a restriction, since we do not investigate topology changes of the membrane. Instead of incorporating the mechanical properties of the IRSp53 cluster as a local spontaneous curvature, we have chosen to model this effect as a constraint (see below). Consequently, the constant bending modulus assumes a homogeneous membrane material.

The tethering energy: The stretching of tethers of barbed ends (slightly) removed from the membrane produces the contribution

$$E_{tether}(t)[\mathscr{M}] := \mu_{tether} \sum_{i \in I_t(t)} d(\mathbf{F}_i(t), \mathscr{M})^2 \tag{2}$$

to the potential energy, where the tethers are assumed to behave like linear springs with spring constant μ_{tether} (see Fig. 1B). By $d(\mathbf{x}, \mathscr{M})$ we denote the signed distance of the point $\mathbf{x} \in \mathbb{R}^3$ to the membrane with the convention that $d(\mathbf{x}, \mathscr{M})$ is positive, when $\mathbf{x}$ is inside the cell. The signed distance is only used for points close to the membrane, where its definition is unambiguous.

Membrane tension: Since the total membrane area of the cell is limited, the protruding lamellipodium has to overcome a membrane tension force, leading to an energy contribution at the rear boundary:

$$E_{pull}(\mathscr{M}^*)[\mathscr{M}] := \mu_{pull} \int_{\Gamma_r^*} \mathbf{r} \cdot \mathbf{a}_n^* \, ds^* \,, \tag{3}$$

where ds is the length element along $\partial\mathscr{M}$ and $\mathbf{a}_n$ is the unit tangent vector of $\mathscr{M}$ normal to $\partial\mathscr{M}$ and oriented inwards. Quantities with the superscript $*$ should not be seen as part of the argument $\mathscr{M}$ of E_{pull}, although they depend on the membrane deformation. By energy minimization (here only with respect to $\mathbf{r}$ in the integrand), E_{pull} contributes the tangential force $-\mu_{pull}\mathbf{a}_n$, distributed along Γ_r (see Fig. 1C). This trick is necessary since such a force is nonconservative and cannot be represented by an energy functional.

Volume constraint: Assuming no mass exchange between the cell and its environment and incompressibility of the cytoplasm, the cell volume remains fixed. The contribution of this constraint to a Lagrangian of the whole cell suggests the energy contribution

$$E_{vol}(\mathscr{M}^*)[\mathscr{M}] := \mu_{vol} \int_{\mathscr{M}^*} \mathbf{r} \cdot \mathbf{n}^* \, d\sigma^* \,, \tag{4}$$

with the unit outward (with respect to the cell) normal $\mathbf{n}$ and the Lagrange multiplier μ_{vol}, whose value has to be prescribed in the absence of information on the remaining part of the cell. The meaning of the superscript $*$ is as in (3). An interpretation of μ_{vol} is the difference between extracellular and intracellular hydrostatic pressures acting on the membrane. Its sign depends on the cytoskeletal activity. If contracting effects, typically caused by actin-myosin interaction, dominate, μ_{vol} will be negative. This is the situation in blebbing cells. On the other hand, dominating protrusion effects, caused by polymerizing filaments pushing the membrane, will be balanced by larger extracellular pressure and make μ_{vol} positive. Here we assume the latter scenario and use small positive values of μ_{vol} (see Fig. 1D). The desired effect is only to keep the membrane in touch with the actin network in regions without tethered filaments. As an alternative, tethering of the cytoskeleton to the membrane would be needed also on the top and the bottom of the lamellipodium.

Constraint 1 – pushing filaments: All barbed ends have to lie inside the cell:

$$d(\mathbf{F}_i(t), \mathscr{M}(t)) \geq 0\,, \qquad i \in I(t)\,, \quad t \geq 0\,, \tag{5}$$

which enforces membrane protrusion, when filaments polymerize at their barbed ends.

Constraint 2 – surface area: We have to make a decision, which piece of membrane we are actually describing. Part of this decision is to fix the surface area:

$$\int_{\mathscr{M}(t)} d\sigma = \int_{\mathscr{M}(0)} d\sigma = A_0\,. \tag{6}$$

Constraint 3 – leading edge: The leading edge region

$$\mathcal{L}(t) = \mathbf{r}(\mathbb{T}^1 \times [L_2/2 - L/2, L_2/2 + L/2], t) \subset \mathscr{M}(t)$$

of the membrane is supported by I-BAR domains of IRSp53 molecules. We assume that they are aligned with the principal direction $\mathbf{c}_2$ of the larger principal curvature k_2, that in the leading edge region this principal direction is equal to the s_2-direction $\partial_{s_2}\mathbf{r}$, and that the larger principal curvature is equal to the curvature $\overline{\kappa}$ of the I-BAR domain. Furthermore, we assume that the leading edge has width L, guaranteed by the constraint that in the leading edge region s_2 is an arclength along the s_2-curves. The parameter L is typically chosen 2–3 times the length of the I-BAR domain, assuming IRSp53 oligomers of that size. The assumption that these oligomers lead to stiffening of the leading edge within the membrane is translated into the

constraint that the center line ($s_2 = L_2/2$) of the leading edge is not curved in the s_2-direction. As formulas, these constraints read

$$\begin{aligned} \mathbf{c}_2 \parallel \partial_{s_2}\mathbf{r}\,, \quad k_2 = \overline{\kappa}\,, \quad |\partial_{s_2}\mathbf{r}| = 1\,, \qquad & \text{for } s_2 \in [L_2/2 - L/2, L_2/2 + L/2]\,, \\ \partial_{s_1}^2\mathbf{r} \parallel \mathbf{n}\,, \qquad & \text{for } s_2 = L_2/2\,. \end{aligned}$$

Constraint 4 – rear boundary: The artificial rear boundary $\Gamma_r(t)$ of the membrane consists of an upper and a lower segment, whose shapes have to be prescribed due to the liquidity of the membrane material. We require that they belong to a cut-off plane, aligned with the x-axis by the periodicity assumptions and roughly orthogonal to the main protrusion direction. This prevents the computed membrane piece from moving completely either to the top or to the bottom of the lamellipodium.

The main protrusion direction in the yz-plane is determined as the average $\omega(t)$ of the azimuth angles

$$\omega_i = \arcsin\left(\frac{f_{iz}}{\sqrt{f_{iy}^2 + f_{iz}^2}}\right)\,, \qquad i \in I_t(t) \cup I_u(t)\,,$$

of growing filaments. The normal vector of the cut-off plane is then given by $\mathbf{d}(t) := (0, \cos(\omega(t)), \sin(\omega(t)))$, and the side condition reads: For each $t \geq 0$ there exists $c(t) \in \mathbb{R}$, such that

$$\mathbf{r}(\mathbf{s}, t) \cdot \mathbf{d}(t) = c(t), \qquad \text{for } \mathbf{s} \in [0, L_1] \times \{0, L_2\}\,. \tag{7}$$

The full membrane model: Denoting the set of all admissible membrane shapes $\mathscr{M}(t) = \mathbf{r}(S, t)$ satisfying the constraints 1–4 by $\mathrm{M}(t)$, the membrane deformation is determined as fixed point of the map $\mathscr{M}^* \mapsto \mathscr{M}$, defined by

$$\begin{aligned} \mathscr{M} &= \operatorname{argmin}_{\hat{\mathscr{M}} \in \mathrm{M}(t)} E(\mathscr{M}^*, t)[\hat{\mathscr{M}}]\,, \\ E(\mathscr{M}^*, t) &:= E_{bend} + E_{tether}(t) + E_{pull}(\mathscr{M}^*) + E_{vol}(\mathscr{M}^*)\,. \end{aligned}$$

More precisely it should be said that it is not guaranteed that the energy functional has a unique minimizer. Therefore we add the requirement that $\mathscr{M}(t)$ should depend continuously on time, when this is true for $E(\mathscr{M}^*, t)$, and that it is chosen as the local minimum closest to $\mathscr{M}(t-)$, when $E(\mathscr{M}^*, t)$ jumps at t.

Actin filaments

Actin filaments are modeled as oriented rods that are immobile and stiff. Uncapped filaments grow continuosly, and nucleation of new filaments by branching off tethered ones is included as stochastic process that happens at barbed ends. After losing its tether a filament gets capped stochastically.

Other effects changing actin filament networks, such as depolymerization and severing, occur predominantly further back in the lamellipodium and are thus neglected. We recall the notation for the filament directions $\mathbf{f}_i$ and the barbed end positions $\mathbf{F}_i(t)$, $i = 1, \ldots, N(t)$, as well as the sets $I_t(t)$, $I_u(t)$ and $I_c(t)$ of indices of respectively tethered, untethered and capped barbed ends, all subsets of $I(t) = \{1, \ldots, N(t)\}$.

Polymerization: For the addition of new monomers at barbed ends, we adopt the actoclampin model [8], which assumes that filaments are elongated with the help of end tracking proteins. The polymerization process involves a motor step, where the barbed end and the membrane are pushed apart, whose activation energy depends on the force between the barbed end and the membrane. The polymerization rate for filament number $i \in I_t(t) \cup I_u(t)$ can be written as

$$k_p = \frac{k_{p,max}}{1 + \exp(\gamma(\mathcal{F}_i - \mathcal{F}_{stall}/2)\delta_i / k_B T)} ,$$

with the force $\mathcal{F}_i$ between the barbed end and the membrane with the convention that positive values of $\mathcal{F}_i$ describe pushing forces and negative values describe pulling forces. The maximal polymerization rate $k_{p,max}$ is thus reached in the limit of large pulling forces. In the case of untethered filaments, which lack a physical link to the membrane, no pulling forces are generated. The thermal energy is denoted by $k_B T$, and $\delta_i = l_f(\mathbf{n} \cdot \mathbf{f}_i)$ is the displacement of the membrane in the direction of the normal $\mathbf{n}$ by adding one monomer, which increases the length of the filament by l_f. The two remaining parameters $\mathcal{F}_{stall}$ and γ are chosen such that the maximal polymerization rate for elongation orthogonal to the membrane ($\delta_i = l_f$) is reached up to a few percent $(1 - \alpha)$ for $\mathcal{F}_i = 0$, and that it is reduced to a few percent α when $\mathcal{F}_i = \mathcal{F}_{stall}$:

$$\gamma = \frac{2 k_B T}{l_f \mathcal{F}_{stall}} \log\left(\frac{1 - \alpha}{\alpha}\right) .$$

The stall force $\mathcal{F}_{stall}$ is chosen in the range 0.5–2 pN, which is rather small compared to published data as an account of the rigidity of the model filaments.

For all tethered barbed ends ($i \in I_t(t)$) located inside the cell (i.e. $d(\mathbf{F}_i(t), \mathscr{M}(t)) > 0$) the force is computed as the pulling force

$$\mathcal{F}_i = -\mu_{tether} d(\mathbf{F}_i(t), \mathscr{M}(t)) .$$

Since untethered filaments lack a connection to the membrane, the pulling force is set to 0. If the barbed end is abutting the membrane (i.e. $d(\mathbf{F}_i(t), \mathscr{M}(t)) = 0$), the momentary value of the total membrane energy $E(t)[\mathscr{M}(t)]$ is compared to the value $E_i(t)[\mathscr{M}_i(t)]$, obtained without the pushing action of

filament number i. This involves the solution of the membrane model with Constraint 1 replaced by

$$d(\mathbf{F}_j(t), \mathscr{M}_i(t)) \geq 0\,, \qquad j \in I(t) \setminus \{i\}\,.$$

The force exerted by the filament (changing the membrane deformation from $\mathscr{M}_i(t)$ to $\mathscr{M}(t)$) is then given by

$$\mathcal{F}_i = \frac{E(t)[\mathscr{M}(t)] - E_i(t)[\mathscr{M}_i(t)]}{d(\mathbf{F}_i(t), \mathscr{M}_i(t))}\,.$$

Branching: A simple model including an exchange of Arp2/3 molecules between the membrane and the cytoplasm, and a branching rate proportional to the local availability of Arp2/3, combined with a Michaelis-Menten approximation [35] leads to the branching rate for filament number $i \in I_t(t)$

$$k_{br,i} = c_{br} a_i = c_{br} \frac{a_0 k_a}{k_a + c_{br}\rho_i}\,,$$

where c_{br} is the branching rate per Arp2/3 density along the membrane, and a_i is the equilibrium Arp2/3 density, written in the Michaelis-Menten approximation in terms of the equilibrium density in the absence of branching, a_0, the attachment/detachment rate of Arp2/3 from the membrane, k_a, and the local density of tethered barbed ends, ρ_i, competing for Arp2/3. The barbed end density ρ_i is computed by the ratio of the number of barbed ends, tethered to a small piece of membrane around $\mathbf{F}_i(t)$, to the area corresponding to the membrane piece. Similar competition terms in the branching rate have been used, e.g. in [28]. The branching rate can be rewritten with conveniently defined parameters as

$$k_{br,i} = \frac{k_{br,max}}{1 + \rho_i L / n_{ref}}\,,$$

with the maximal branching rate $k_{br,max} = c_{br} a_0$ and a typical number $n_{ref} = k_a L / c_{br}$ of barbed ends per length of leading edge. Motivated by results of [63], showing distances between branch points on filaments larger than their helical pitch, we assume a minimal distance l_{br} between branch points.

When branching occurs from filament number i, the direction $\mathbf{f}_d$ of the daughter filament needs to be determined. Since we assume a fixed branching angle ϕ_{br}, $\mathbf{f}_d$ needs to lie on a cone, determined by

$$\mathbf{f}_i \cdot \mathbf{f}_d = \cos\phi_{br}\,.$$

On this cone, the branching direction is chosen randomly. The choice of the preferred directions is one of the main new modeling assumptions of

this work. As described in Constraint 3, we assume the I-BAR domains of IRSp53 to be aligned with the direction of the bigger principal curvature of the membrane. Furthermore the IRSp53 molecules line up side-by-side, i.e. in the direction $\partial_{s_1}\mathbf{r}$. This makes it natural to assume that $\partial_{s_1}\mathbf{r}$ provides the preferred branching direction in the sense that the direction $\mathbf{f}_d$ of the daughter filament lies in the plane spanned by the mother filament direction $\mathbf{f}_i$ and $\xi = \partial_{s_1}\mathbf{r}/|\partial_{s_1}\mathbf{r}|$. The intersection of the cone and the plane leads to two possible preferred directions, which can be written as

$$\mathbf{f}_d^{\pm} = \frac{\sin(\phi_i \mp \phi_{br})\mathbf{f}_i \pm \sin(\phi_{br})\xi}{\sin(\phi_i)}\,, \quad \text{with } \cos(\phi_i) = \mathbf{f}_i \cdot \xi\,.$$

The above mentioned cone can now be parametrized by an angle ϕ:

$$\mathbf{f}_d(\phi) = \cos(\phi)\mathbf{f}_d^{+} + (1-\cos(\phi))\cos(\phi_{br})\mathbf{f}_i + \frac{\sin(\phi)\sin(\phi_{br})}{\sin(\phi_i)}\mathbf{f}_i \times \xi\,,$$

such that $\mathbf{f}_d(0) = \mathbf{f}_d^{+}$, $\mathbf{f}_d(\pi) = \mathbf{f}_d^{-}$. We restrict to daughter filaments pointing towards the membrane and not too parallel to it by requiring

$$\mathbf{f}_d(\phi) \cdot \mathbf{n} \geq \sin(\phi_{min}) \quad \Longleftrightarrow \quad \phi \in D_{min}\,,$$

with the unit outward normal $\mathbf{n}$ to the membrane and a cut-off angle ϕ_{min}. The condition $\phi_{min} < \pi/2 - \phi_{br}$ is sufficient to guarantee that at least one of the preferred daughter filament directions lies in the allowed part of the cone. The daughter filament direction is now determined by a random choice of $\phi \in D_{min}$ according to the probability density

$$g(\phi) = \frac{1}{c}\left(\frac{1-\cos(\phi_i)}{2} g_0\left(\frac{\phi}{\sigma_{br}}\right) + \frac{1+\cos(\phi_i)}{2} g_0\left(\frac{\phi-\pi}{\sigma_{br}}\right)\right)\,, \qquad (8)$$

where g_0 is the normalized Gaussian on $[-\pi/\sigma_{br}, \pi/\sigma_{br}]$ and continued periodically outside. The positive constant c is chosen such that g is a probability density on D_{min}. The weights involving ϕ_i give preference to daughter filaments pointing more towards the membrane (see Fig. 2).

Breaking tethers: There are two possible reasons for breaking the connection of filament number i with the membrane. The first one is $\mathcal{F}_i = \mu_{tether} d(\mathbf{F}_i(t), \mathscr{M}(t)) > \mathcal{F}_{max}$, i.e. when the force on the tether exceeds a critical value. Secondly tethers are lost if the barbed end grows out of the IRSp53 cluster due to lateral or vertical flow. Untethered filaments are still polymerizing but without any pulling forces, and they are unable to form branches.

Capping: Untethered barbed ends are capped randomly with the rate p_{cap}. This process is motivated by the lack of protection from capping by a barbed end tether. Capped filaments do not grow or branch anymore and influence the membrane only as obstacles.

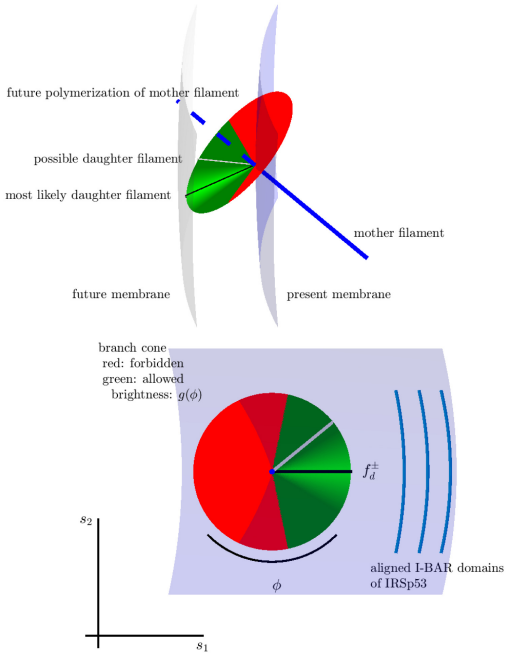

Figure 2: Branching, two views. To indicate the direction of movement, the membrane is depicted at time t in light blue and at time $t+\Delta t$ in grey; motherfilament in blue; extrapolated motherfilament in dashed blue; most likely and a second possible daughter filament direction in black and, respectively, grey. The lower view is in the direction of the motherfilament highlighting the different regions of the branching cone: directions pointing backwards in light red, directions too parallel to the membrane in dark red and the allowed part of the branching cone in shaded green, the lighter color indicating a higher probability to branch in that direction. Also indicated is the assumed positioning of the I-BAR domains of IRSp53 molecules.

Lateral boundaries: Just as the membrane, the filaments are assumed to satisfy periodic boundary conditions, meaning that filaments growing out of the simulation domain through one of the planes $r_1 = 0$ or $r_1 = x_{max}$, immediately enter again through the other one at the same (r_2, r_3)-position and with the same direction.

Initial conditions: The initial condition is constructed to resemble a typical shape for a protruding lamellipodium of thickness H_0. The initial barbed ends $\mathbf{F}_i(0)$ ($i \in I_0 = \{1, \ldots, N_0\}$, $N_0 = n_{ref} x_{max}$) are randomly placed on a cylindric surface orthogonal to the x-direction, consistent with the Constraints 2–4 for the simulated membrane piece.

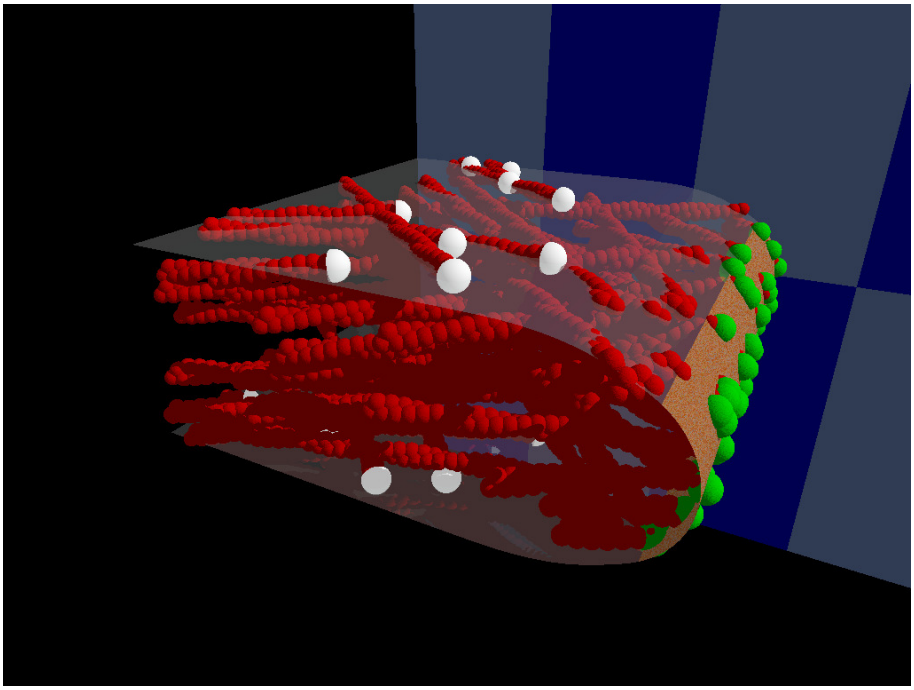

Figure 3: Typical initial condition for the simulation; barbed ends of capped filaments are depicted in white

For the filament directions

$$\mathbf{f}_i = \begin{pmatrix} \cos(\phi_i)\cos(\gamma_i) \\ \sin(\phi_i)\cos(\gamma_i) \\ \sin(\gamma_i) \end{pmatrix},$$

the angles ϕ_i and γ_i are chosen randomly with a two-peaked distribution for ϕ_i, where the peaks are at $\pi/2 \pm \phi_{br}/2$ with standard deviation σ_ϕ. The azimuth angles γ_i are chosen with mean 0 and standard deviation σ_γ (see Fig. 3).

Numerical implementation

The numerical implementation of the model is described in detail by the same authors in [53]. The time stepping is based on operator splitting separating the adjustment of the cell membrane and the evolution of the filaments. The membrane is approximated by a Loop subdivision surface [31], based on a triangulation of the parameter domain, a finite element method already successfully used to model cell membranes in [16]. The constraints are replaced by penalty terms, leading to an unconstrained minimization problem. At each time step the minimizing surface is found as steady state

of the corresponding gradient flow, starting from the position of the membrane at the previous time step. Thus we ensure that a local minimum near the previous configuration is attained. In the second part the rates for polymerization, branching and capping are determined for each filament, and they are evolved accordingly by a Monte Carlo procedure.

Choice of parameter values

Symbol	Value	Description	Refs.
x_{max}	250nm	minimal length of simulated leading edge	
A_0	$1.4 \times 10^5 \text{nm}^2$	area of simulated membrane	
L	75nm	leading edge width (supported by IRSp53)	
μ_{bend}	$20 k_B T \approx 82\,\text{pN nm}$	membrane bending modulus (at $T = 300\text{K}$)	[4, 14]
μ_{tether}	$1\,\text{pN/nm}$	tether spring constant	[42]
μ_{pull}	5×10^{-3}–10^{-1}pN/nm	membrane tension at the rear	
μ_{vol}	10^{-5}pN/nm^2	pressure on the membrane	
$\overline{\kappa}$	$(40\text{nm})^{-1}$	IRSp53 I-BAR domain curvature	[29, 36]

Table 1: Membrane geometry and mechanical parameters

Symbol	Value	Description	Refs.
$k_{p,max}$	15s^{-1}	maximal polymerization rate	[8]
$\mathcal{F}_{stall}$	1.5pN	polymerization stall force	[17]
$k_B T$	4.1pN nm	thermal energy (at $T = 300\text{K}$)	
l_f	2.7nm	elongation length per monomer	[57]
α	0.01	reduction factor of the maximal polymerization rate at the stall force	
$k_{br,max}$	$(10\text{s})^{-1}$	maximal branching rate	
n_{ref}	$140\mu\text{m}^{-1}$	reference number of barbed ends per leading edge length	[48]
l_{br}	10nm	minimal distance between branches	[63]
ϕ_{br}	73°	branching angle	[63]
ϕ_{min}	15°	minimal angle between filament and membrane	
σ_{br}	10°	standard deviation of branching direction	
p_{cap}	0.16–0.5s^{-1}	capping rate for untethered filaments	
$\mathcal{F}_{max}$	10pN	maximal tether force	[60]

Table 2: Polymerization, branching, and capping parameters

The parameters important for the membrane model are collected in Ta-

ble 1. The width x_{max} (in the direction of the leading edge) of the simulation region is chosen as a compromise between the goals to permit a reasonably large number of filaments and of computational efficiency, and a similar argument holds for the choice of the total simulated membrane area A_0. No experimental evidence is available for the choice of the width L of the leading edge region. There is some indirect evidence [51] that I-BAR domains (of length 18nm [58]) may oligomerize by end-to-end connections. We choose a value of L, approximately corresponding to oligomers with 4 members. The membrane curvature radius induced by the I-BAR domain of IRSp53 is approximately $1/\overline{\kappa} = 40$nm [29, 36]. The bending modulus of the membrane depends on its detailed composition. Our choice $\mu_{bend} = 20k_BT$ for its value is of the correct order of magnitude [4, 14]. The spring constant of tethers connecting barbed ends to the membrane is another parameter, where good experimental evidence is missing. The value $\mu_{tether} = 1$pN/nm has been suggested in [9] and is of the same order of magnitude as in simulations of the actin comet tail of baculovirus [42], where it produced reasonable results. Our standard value for the membrane tension $\mu_{pull} = 5 \times 10^{-3}$pN/nm applied at the rear end of the simulated membrane is rather on the floppy side (compare to, e.g. [39]), corresponding to a rather small value of the polymerizaton stall force (see below). Some experiments with (up to 20 fold) higher values of the membrane tension have also been carried out. The value μ_{vol} of the inward pressure on the membrane is chosen such that a total force of only a few pN acts over the whole simulated membrane area, which just prevents the membrane from lifting off from the actin network in regions without tethered filament ends. This has a negligible effect on the lamellipodium geometry.

Table 2 contains the parameters corresponding to polymerization, branching, and capping. The value of the maximal polymerization rate $k_{p,max} = 15/$s has been chosen such that a maximal cell speed of 2μm/min [63] is reached by filaments with an angle of $\phi_{br}/2$ to the leading edge. This value of $k_{p,max}$ lies within a range given in [8]. The polymerization stall force $\mathcal{F}_{stall}$ is a disputed parameter. The value we have picked from the literature [17] is on the small side, as mentioned above. Our precise definition of stall force is the force, where the maximal polymerization rate is reduced by the factor $\alpha = 0.01$, whose precise choice is not very important. The maximal branching rate $k_{br,max}$ is used as a fitting parameter to regulate the total number of pushing filaments per leading edge length, which is well know to be of the order of $100/\mu$m (see, e.g. [48]), also motivating our choice $n_{ref} = 140/\mu$m. A minimal distance l_{br} between branches on a filament is motivated by the observation that very few branches are closer to each other than the helical repeat (≈ 36nm) of actin filaments [63]. We choose a minimal distance smaller than that to allow for the influence of membrane deformations or filament twisting. The minimal angle ϕ_{min} between nucleated filaments and the membrane prohibits the creation of filaments without

a chance of staying attached to the membrane. Its value is an ad-hoc choice, just as that of the standard deviation σ_{br} of the branching direction from the preferred one. The latter determines the number of filaments, whose barbed ends eventually become untethered by leaving the leading edge region. No experimental evidence is available for the capping rate p_{cap} of these filaments. Together with the width L of the leading edge region, this is the parameter expected to have the strongest influence on the lamellipodium width. Different choices for its value in a reasonable range have been tested. The maximal pulling force $\mathcal{F}_{max}$, which can be sustained by a tether, has been measured in [60].

Reasonably realistic initial networks of $N_0 = n_{ref}x_{max}$ filaments are determined stochastically using the parameters in Table 3. Different values for the initial thickness H_0 of the lamellipodium have been tested.

Symbol	Value	Description	Refs.
H_0	100–300nm	lamellipodium thickness	[56]
σ_ϕ	10°	standard deviation of horizontal filament angle	[66]
σ_γ	5°	standard deviation of azimuth filament angle	[49]

Table 3: Initial condition parameters

3 Simulation results

All simulations have been carried out for a time of 2 minutes with time steps of 20ms. The description of the simulation results is grouped into three parts, dealing with a qualitative description of computed membrane deformations, with the comparison to experimental data for our standard parameter set with $p_{cap} = 0.2\text{s}^{-1}$, $\mu_{pull} = 5 \times 10^{-3}$pN/nm, and with the effects of variations of these two parameters, respectively.

The simulated lamellipodium is flat

The most important geometric observation is that we are able to simulate pieces of lamellipodium protruding for at least 3μm in a stable manner and remaining flat even without adhesion to a substrate. As an example, Fig. 4 and the video in the supporting material show a typical time evolution and Fig. 5 gives a perspective from the side. The top and bottom parts of the cell membrane remain very flat apart from the necessary bending near the leading edge. The designated leading edge region stays at the front of the lamellipodium, a property not a priori enforced by the model. The membrane stiffness is sufficient to keep the leading edge rather straight. As will be further developed in the quantitative part of the results, the mean thickness of the lamellipodium evolves around an equilibrium.

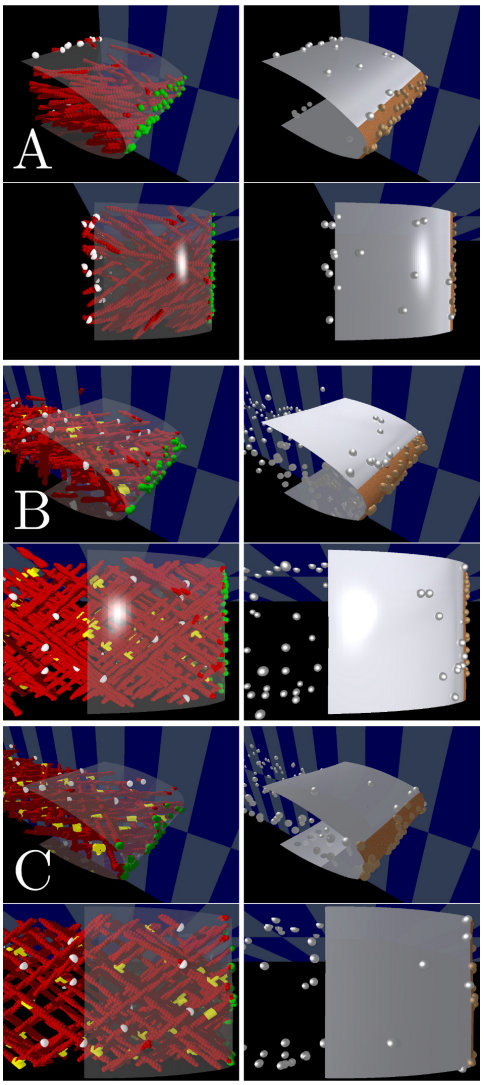

Figure 4: Time evolution after A: 0s, B: 60s, and C: 120s. Left column: Filaments in red, tethered barbed ends in green, capped barbed ends in white, and branch points in yellow. Right column: Membrane in silver with leading edge region in brown, pushing barbed ends indicated on the membrane surface as bronze (tethered barbed ends) or silver (untethered or capped filaments) spheres.

Quantitative results

Thickness: The thickness of the simulated lamellipodium at time t is computed as the mean of the distances between corresponding points on the upper and the lower rear boundary. For each value $x \in [0, x_{max}]$ there exists exactly one point $\mathbf{r}_l(x,t)$ on the lower part of $\Gamma_r(t)$ ($s_2 = 0$) and one, $\mathbf{r}_u(x,t)$, on the upper part ($s_2 = L_2$) with $r_{l1}(x,t) = r_{u1}(x,t) = x$. The

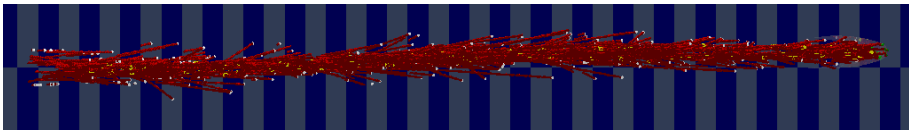

Figure 5: Side view of the simulation after 120s shows the flatness of the lamellipodium.

lamellipodium thickness is then defined by

$$H(t) := \frac{1}{x_{max}} \int_0^{x_{max}} |\mathbf{r}_l(x,t) - \mathbf{r}_u(x,t)|\, dx\,.$$

Figs. 6A, 6B, 6C show the time evolutions of the thickness for 6 simulation runs each for the initial thicknesses 100nm, 160nm, and, respectively, 300nm. The ensemble averages of these simulations are shown in Fig. 6D. An even clearer picture is obtained by time averaging of these curves over the previous 50sec, Fig. 6E. The mean thickness settles around approximately 147nm, which is in the range of measured data reported between 70nm and 180nm (see, e.g., [25]). The stochastic variations are to be expected and within a reasonable range. The variations of the initial thickness does no influence the average thickness in the long run. The mean thickness of 147nm seems to be a stable equilibrium value for our standard parameter set.

Speed: The average protrusion speed in our simulations is 1.8μm/min, close to the one used for the computation of the maximal polymerization rate.

Filaments: For key properties of the simulated actin filament network long term averages after an initial transient period have been computed and compared to data from the literature. We obtained the average values:

- 88 for the number of tethered filaments per micron (Fig. 7A), which is on the low side compared to Vic Small's estimate of around 120 filaments per micron [48],
- $134\mu\text{m}^{-1}$ for the F-actin density (Fig. 7B, again rather low compared to the value $342\mu\text{m}^{-1}$, extracted from electron tomograms by filament tracking [66]), and
- $205/\mu\text{m}^2$ for the branch density (Fig. 7C, comparing well to the one reported for RAC induced lamellipodia, approximately $240/\mu\text{m}^2$ [26]).

Considering that no specific cell type has been modelled, that the experimental data originate from rather different experimental set-ups, and that no

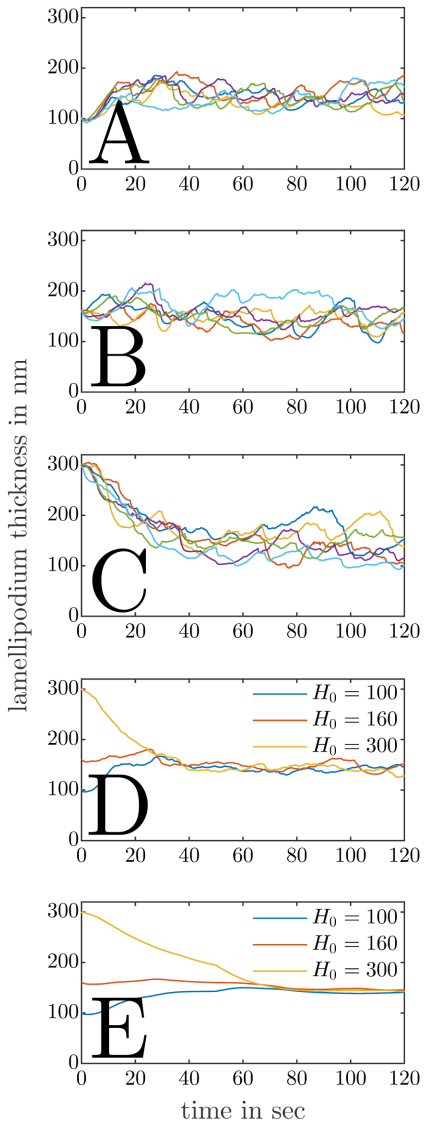

Figure 6: Lamellipodium thickness vs. time. A, B, C: 6 simulations each with, respectively, 100nm, 160nm, and 300nm initial thickness. D: averages of the simulations in A, B, and C. E: time averages of the ensemble averages in D over the previous 50sec.

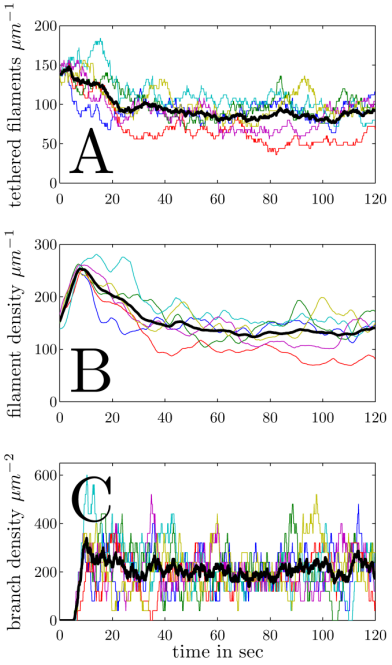

Figure 7: Properties of the actin filament network in the six simulations of Fig. 6A. A: number of tethered filaments, B: filament density (length/area), C: branch density (number/area); average in black.

thorough parameter fitting procedure has been carried out, all the extracted data fit the reported values reasonably well.

The angular distribution of filaments in the protrusion plane shows two peaks at a distance of half the branching angle around the direction of protrusion (Fig. 8), as typical for protruding cells. The peaks are too pronounced compared to electron tomograms [27, 66], possibly due to the rigidity of the simulated filaments and the branches.

As an indication for the main protrusion direction, we use the mean azimuth angle of all polymerizing filaments (see Constraint 4). Fig. 9 shows that the mean protrusion direction is on the average preserved with time, with slightly varying averages in different simulation runs as a consequence of not prescribing the protrusion direction.

Influence of varying parameters

The effect of varying the capping rate p_{cap} for untethered filaments is depicted in Fig. 10. The tendency is not surprising: Bigger values of the capping rate lead to smaller values and smaller fluctuations of the lamel-

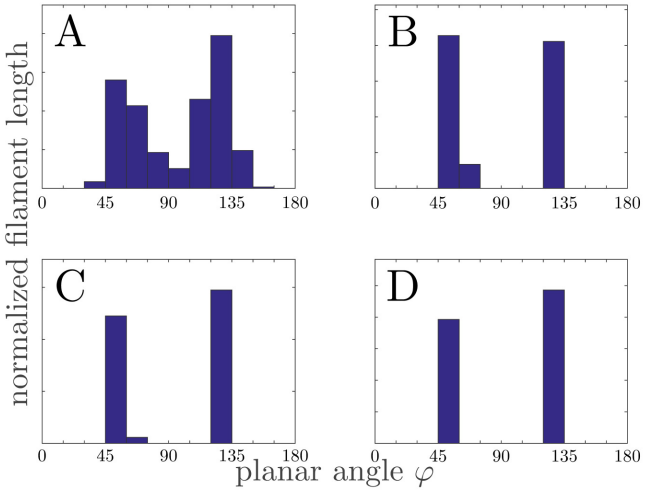

Figure 8: Angle distribution of one simulation over time after A: 0s, B: 40s, C: 80s, D: 120s (normalized filament length per angle).

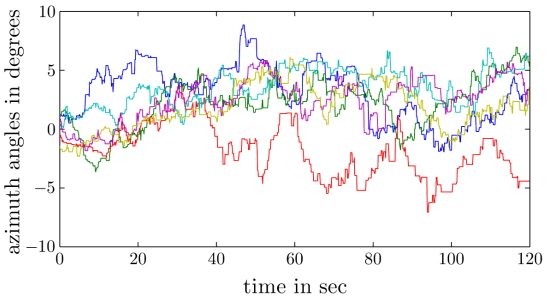

Figure 9: Average azimuth angle ω over time.

lipodium thickness. For small capping rates a linear dependence could be expected, with a saturation effect for large capping rates, whence the width of the IRSp53 cluster will be the dominating influence.

Finally, we carried out a number of experiments with higher values (2–20 fold of the standard value) of the membrane tension parameter. This slightly reduces the mean values of the lamellipodium thickness, but most notably its variance depending on time is reduced (Fig. 11A). Both filament density and branch density increase with membrane tension (Fig. 11B,C) which is a natural consequence of smaller polymerization speed at roughly unchanged branching rates.

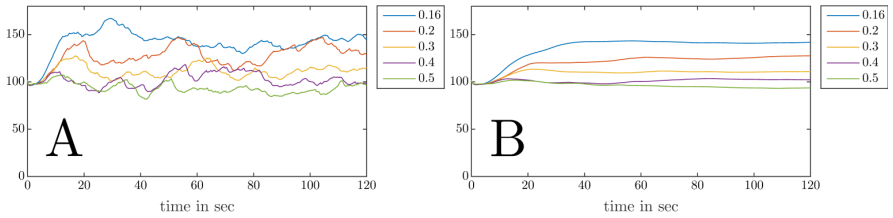

Figure 10: A: Influence on the lamellipodium thickness of varying the capping rate p_{cap}. B: time averages.

4 Discussion

This work tries to give partial answers to the question, why flat lamellipodia exist. The main goal was to develop a theory based on protein interactions using only local information without any prescribed input on global quantities such as protrusion direction or lamellipodium thickness. The essential idea is a mutual influence between local geometric properties of the cell membrane and the dynamics of the actin network, mediated by membrane bound proteins. A reasonable candidate for this role is IRSp53, whose membrane bound I-BAR domain interacts with membrane curvature and whose SH3 domains may act as an anchor for promotors of actin branching and polymerization.

In our mathematical model for actin dynamics and membrane deformation, the presence of a band-shaped cluster of IRSp53 molecules attached to the cell membrane and inducing membrane curvature is assumed. Only in this aggregated form, IRSp53 can be expected to have significant influence on membrane bending. The positioning of the cluster is part of the energy minimization procedure determining membrane shape. The important question of describing the aggregation mechanism producing the cluster has not been addressed. It would require a model for the movement of IRSp53 molecules along a deforming membrane. This is a major step in model development requiring a description of the incompressible lipid flow along the membrane [21] as a prerequisite. A computationally feasible approach, which does not seem to be available yet, is subject of our ongoing work. The model presented here may explain the stability of flat lamellipodia (see Fig. 6), but not their initiation.

Another challenge remaining open so far, is a full parametrization of the model by fitting to experimental results, including a systematic study of sensitivities with respect to critical parameters. Since filament tracking and the identification of branch points in electron tomograms [63] provides complete snap shots of the actin network, the complete parametrization (simi-

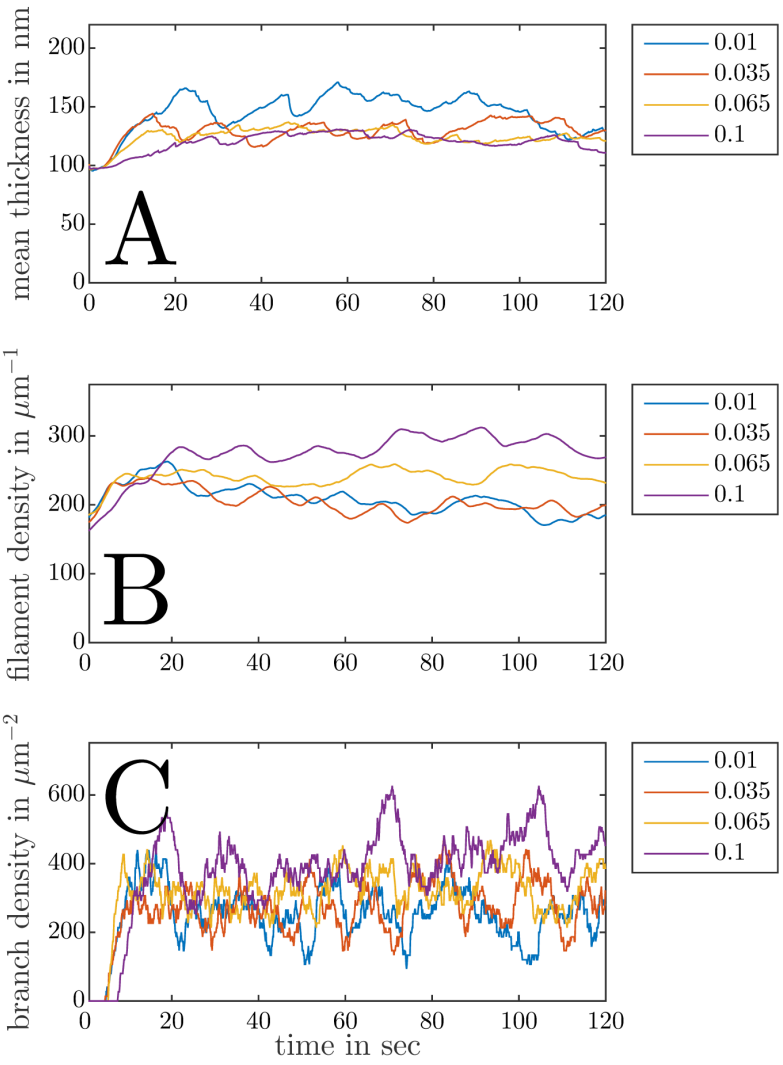

Figure 11: Influence of increased membrane tension on A: lamellipodium thickness, B: filament density, and C: branch density.

larly to [42]) is a realistic goal. The bottleneck in this effort is computation time. Our numerical methods [53] need to be optimized, such that many simulation runs can be done within acceptable periods of time.

Acknowledgment

This work has been supported by the Vienna Science and Technology Fund under grants no. MA09-004 and LS13-029. The authors also acknowledge many hours of enlightening discussions with Vic Small and Michael Sixt and members of their groups.

References

[1] B. Alberts, A. Johnson, J. Lewis, M. Raff, K. Roberts, and P. Walter. *Molecular Biology of the Cell*. Garland Science, fourth edition, 2002.

[2] E. Atilgan, D. Wirtz, and S. X. Sun. Morphology of the Lamellipodium and Organization of Actin Filaments at the Leading Edge of Crawling Cells. *Biophys J.*, 89:3589–3602, 2005.

[3] J. R. Bamburg and B. W. Bernstein. Roles of ADF/cofilin in actin polymerization and beyond. *F1000 Biol. Rep.*, 2, 2010.

[4] D. Boal. *Mechanics of the Cell*. Cambridge University Press, 2002.

[5] C. Chaponnier, P. A. Janmey, and H. L. Yin. The Actin Filament-severing Domain of Plasma Gelsolin. *J. Cell Biol.*, 103:1473–1481, 1986.

[6] W. Cho and R. V. Stahelin. Membrane-Protein Interactions in Cell Signaling and Membrane Trafficking. *Annu. Rev. Bioph. Biom.*, 34(1):119–151, 2005.

[7] L. P. Cramer. Molecular mechanism of actin-dependent retrograde flow in lamellipodia of motile cells. *Front. Biosci*, (2):260–270, 1997.

[8] R. B. Dickinson. A Multi-Scale Mechanistic Model for Actin-Propelled Bacteria. *Cell. Mol. Bioeng.*, 1(2-3):110–121, 2008.

[9] R.B. Dickinson. Models for actin polymerization motors. *J. Math. Biol.*, 58:81–103, 2009.

[10] R.B. Dickinson, L. Caro, and D.L. Purich. Force generation by cytoskeletal filament end-tracking proteins. *Biophys. J.*, 87:2838–2854, 2004.

[11] R.B. Dickinson and D.L. Purich. Clamped-filament elongation model for actin-based motors. *Biophys. J.*, 82:605–617, 2002.

[12] M. Edidin. Lipids on the frontier: a century of cell-membrane bilayers. *Nat. Rev. Mol. Cell Biol.*, 4:414–418, 2003.

[13] M. Enculescu, M. Sabouri-Ghomi, G. Danuser, and M. Falcke. Modeling of Protrusion Phenotypes Driven by the Actin-Membrane Interaction. *Biophys. J.*, 98:1571–1581, 2010.

[14] E. Evans and W. Rawicz. Entropy-Driven Tension and Bending Elasticity in Condensed-Fluid Membranes. *Phys. Rev. Lett.*, 64(17):2094–2097, 1990.

[15] P. F. Fahey and W. W. Webb. Lateral Diffusion in Phospholipid Bilayer Membranes and Mulitlamellar Liquid Crystals. *Biochemistry*, 17:3046–3053, 1978.

[16] F. Feng and W. S. Klug. Finite element modeling of lipid bilayer membranes. *J. Comput. Phys.*, 220:394–408, 2006.

[17] M. J. Footer, J. W. J. Kerssemakers, J. A. Theriot, and M. Dogterom. Direct measurement of force generation by actin filament polymerization using an optical trap. *P. Natl. Acad. Sci. USA*, 104(7):2181–2186, 2007.

[18] F. Gittes, B. Mickey, J. Nettleton, and J. Howard. Flexural Rigidity of Microtubules and Actin Filaments Measured from Thermal Fluctuations in Shape. *J. Cell Biol.*, 120(4):923–934, 1993.

[19] W. Helfrich. Elastic Properties of Lipid Bilayers: Theory and Possible Experiments. *Z. Naturforsch. C*, 28:693–703, 1973.

[20] K. C. Holmes, D. Popp, W. Gebhard, and W. Kabsch. Atomic model of the actin filament. *Nature*, 347:44–49, 1990.

[21] D. Hu, P. Zhang, and W. E. Continuum theory of a moving membrane. *Phys. Rev. E*, 75:041605, 2007.

[22] L. Hu and G. A. Papoian. Mechano-Chemical Feedbacks Regulate Actin Mesh Growth in Lamellipodial Protrusions. *Biophys. J.*, 98:1375–1384, 2010.

[23] G. E. Jones. Cellular signaling in macrophage migration and chemotaxis. *J. Leukocyte Biol.*, 68(5):593–602, 2000.

[24] R. Keller. Cell migration during gastrulation. *Curr. Opin. Genet. Dev.*, 17(5):533 – 541, 2005.

[25] S. A. Koestler, K. Rottner, F. Lai, J. Block, M. Vinzenz, and J. V. Small. F- and G-Actin Concentrations in Lamellipodia of Moving Cells. *PLOS ONE*, 4.

[26] S. A. Koestler, A. Steffen, M. Nemethova, M. Winterhoff, N. Luo, and J. M. etal. Holleboom. Arp2/3 complex is essential for actin network treadmilling as well as for targeting of capping protein and cofilin. *Mol. Biol. Cell*, 24:2861 – 2875, 2013.

[27] S.A. Koestler, S. Auinger, M. Vinzenz, K. Rottner, and J.V. Small. Differentially oriented populations of actin filaments generated in lamellipodia collaborate in pushing and pausing at the cell front. *Nat. Cell. Biol.*, 10(3):306–313, 2008.

[28] C. I. Lacayo, Z. Pincus, M. M. VanDuijn, C. A. Wilson, D. A. Fletcher, F. B. Gertler, A. Mogilner, and J. A. Theriot. Emergence of Large-Scale Cell Morphology and Movement from Local Actin Filament Growth Dynamics. *PLOS Biol.*, 5:e233, 2007.

[29] M. A. Lemmon. Membrane recognition by phospholipid-binding domains. *Nat. Rev. Mol. Cell Biol.*, 9:99–111, 2008.

[30] A. Locascio and M. A. Nieto. Cell movements during vertebrate development: integrated tissue behaviour versus individual cell migration. *Curr. Opin. Genet. Dev.*, 11(4):464 – 469, 2001.

[31] C. Loop. Smooth Subdivision Surfaces Based on Triangles. Master's thesis, University of Utah, 1987.

[32] L. M. Machesky. Lamellipodia and filopodia in metastasis and invasion. *FEBS Lett.*, 582(14):2102 – 2111, 2008.

[33] L. M. Machesky and R. H. Insall. Scar1 and the related Wiskott-Aldrich syndrome protein, WASP, regulate the actin cytoskeleton through the Arp2/3 complex. *Curr. Biol.*, 8:1347–1356, 1998.

[34] C. R. Mackay. Moving targets: cell migration inhibitors as new anti-inflammatory therapies. *Nat. Immunol.*, 9:988–998, 2008.

[35] A. Manhart, D. Oelz, C. Schmeiser, and N. Sfakianakis. An Extended Filament Based Lamellipodium Model Produces Various Moving Cell Shapes in the Presence of Chemotactic Signals. Preprint, 2015.

[36] P. K. Mattila, A. Pykäläinen, J. Saarikangas, V. O. Paavilainen, H. Vihinen, E. Jokitalo, and P. Lappalainen. Missing-in-metastasis and IRSp53 deform PI(4,5)P2-rich membranes by an inverse BAR domain-like mechanism. *J. Cell Biol.*, 176:953–964, 2007.

[37] C. T. Mierke, D. Roesel, B. Fabry, and J. Brabek. Contractile forces in tumor cell migration. *Eur. J. Cell Biol.*, 87(8):669–676, 2008.

[38] C. Mim and V. M. Unger. Membrane curvature and its generation by BAR proteins. *Trends Biochem. Sci.*, 37(12):526 – 533, 2012.

[39] A. Mogilner and G. Oster. Cell motility driven by actin polymerization. *Biophys. J.*, 71(6):3030–3045, 1996.

[40] A. Mogilner and G. Oster. Force generation by actin polymerization ii: The elastic ratchet and tethered filaments. *Biophys. J.*, 84:1591–1605, 2003.

[41] J. Müller. Baculovirus-induced Actin Comet Tails: Structure of the Propulsion Machinery. Master's thesis, University of Vienna, 2012.

[42] J. Müller, J. Pfanzelter, C. Winkler, A. Narita, C. Le Clainche, M. Nemethova, M. Carlier, Y. Maeda, M. D. Welch, T. Ohkawa, C. Schmeiser, G. P. Resch, and J. V. Small. Electron Tomography and Simulation of Baculovirus Actin Comet Tails Support a Tethered Filament Model of Pathogen Propulsion. *PLOS Biol.*, 12, 2014.

[43] H. Nakagawa, H. Miki, M. Nozumi, T. Takenawa, S. Miyamoto, J. Wehland, and J. V. Small. IRSp53 is colocalized with WAVE2 at the tips of protruding lamellipodia and filopodia independently of Mena. *J. Cell Sci.*, 116:2577–2583, 2003.

[44] M. O'Donnell, R. K. Chance, and G. J. Bashaw. Axon Growth and Guidance: Receptor Regulation and Signal Transduction. *Annu. Rev. Neurosci.*, 32(1):383–412, 2009.

[45] D. Oelz and C. Schmeiser. Simulation of lamellipodial fragments. *J. Math. Biol.*, 64:513–528, 2012.

[46] G. M. O'Neill. The coordination between actin filaments and adhesion in mesenchymal migration. *Cell Adh. Migr.*, 3:355–357, 2009.

[47] T. D. Pollard and J. A. Cooper. Actin, a Central Player in Cell Shape and Movement. *Science*, 326(5957):1208–1212, 2009.

[48] M. Prass, K. Jacobson, A. Mogilner, and M. Radmacher. Direct measurement of the lamellipodial protrusive force in a migrating cell. *J. Cell Biol.*, 174:767–772, 2006.

[49] A. Rigort, D. Günther, R. Hegerl, D. Baum, B. Weber, Prohaska S., O. Medalia, W. Baumeister, and H. Hege. Automated segmentation of electron tomograms for a quantitative description of actin filament networks. *J. Struct. Biol.*, 177(1):135 – 144, 2012.

[50] B. Rubinstein, M. F. Fournier, K. Jacobson, A. B. Verkhovsky, and A. Mogilner. Actin-Myosin Viscoelastic Flow in the Keratocyte Lamellipod. *Biophys. J.*, 97:1853–1863, 2009.

[51] J. Saarikangas, H. Zhao, A. Pykäläinen, P. Laurinmäki, P. K. Mattila, Kinnunen P. K., S. J. Butcher, and Lappalainen P. Molecular Mechanisms of Membrane Deformation by I-BAR Domain Proteins. *Curr. Biol.*, 19(2):95 – 107, 2009.

[52] T. E. Schaus, E. W. Taylor, and G. G. Borisy. Self-organization of actin filament orientation in the dendritic-nucleation/array-treadmilling model. *P. Natl. Acad. Sci. USA*, 104(17):7086–7091, 2007.

[53] C. Schmeiser and C. Winkler. A finite element method for cell membranes with tethered obstacles. Preprint, 2015.

[54] C. H. Schreiber, M. Stewart, and T. Duke. Simulation of cell motility that reproduces the force-velocity relationship. *P. Natl. Acad. Sci. USA*, 2010.

[55] G. Scita, S. Confalonieri, P. Lappalainen, and S. Suetsugu. IRSp53: crossing the road of membrane and actin dynamics in the formation of membrane protrusions. *Trends Cell Biol.*, 18:52–60, 2008.

[56] J. V. Small, T. Stradal, E. Vignal, and K. Rottner. The lamellipodium: where motility begins. *Trends Cell Biol.*, 12:112–120, 2002.

[57] T. Splettstoesser, K. C. Holmes, F. Noé, and J. C. Smith. Structural Modeling and Molecular Dynamics Simulation of the Actin Filament. *Proteins*, 79(7):2033–2043, 2011.

[58] A. Suarez, T. Ueno, R. Huebner, J.M. McCaffery, and T. Inoue. Bin/amphiphysin/rvs (bar) family members bend membranes in cells. *Sci. Rep.*, 4:4693, 2014.

[59] Y. Tseng, T. P. Kole, J. S. H. Lee, E. Fedorov, S. C. Almo, B. W. Schafer, and D. Wirtz. How actin crosslinking and bundling proteins cooperate to generate an enhanced cell mechanical response. *Biochem. Bioph. Res. Co.*, 334(1):183 – 192, 2005.

[60] A. Upadhyaya, J. R. Chabot, A. Andreeva, A. Samadani, and A. van Oudenaarden. Probing polymerization forces by using actin-propelled lipid vesicles. *P. Natl. Acad. Sci. USA*, 100(8):4521–4526, 2003.

[61] E. Urban, S. Jacob, M. Nemethova, G. P. Resch, and J. V. Small. Electron tomography reveals unbranched networks of actin filaments in lamellipodia. *Nat. Cell. Biol.*, 12:429–435, 2010.

[62] G. van Meer, D. R. Voelker, and G. W. Feigenson. Membrane lipids: where they are and how they behave. *Nat. Rev. Mol. Cell Biol.*, 9:112–124, 2008.

[63] M. Vinzenz, M. Nemethova, F. Schur, J. Mueller, A. Narita, E. Urban, C. Winkler, C. Schmeiser, S. Koestler, K. Rottner, G. Resch, Y. Maeda, and J. V. Small. Actin branching in the initiation and maintenance of lamellipodia. *J. Cell Sci.*, 125:2775–2785, 2012.

[64] A. Weeds and S. Maciver. F-actin capping proteins. *Curr. Opin. Cell Biol.*, 5(1):63 – 69, 1993.

[65] A. Wegner. Head to Tail Polymerization of Actin. *J. Mol. Biol.*, 108:139–150, 1976.

[66] C. Winkler, M. Vinzenz, J. V. Small, and C. Schmeiser. Actin filament tracking in electron tomograms of negatively stained lamellipodia using the localized radon transform. *J. Struct. Bio.*, 178(1):19 – 28, 2012.

[67] D. Yates. Axon growth: Separating growth from regrowth. *Nat. Rev. Neurosci.*, 13:668–669, 2012.

[68] S. H. Zigmond and S. J. Sullivan. Sensory adaptation of leukocytes to chemotactic peptides. *J. Cell Biol.*, 82:517–527, 1979.